University of Hertfordshire UH 25 Research Archive

Citation for published version:
S. Kaviraj, et al., "The triggering of local AGN and their role in regulating star formation", *Monthly Notices of the Royal Astronomical Society,* Vol. 452(1): 774-783, July 2015.

DOI:
https://doi.org/10.1093/mnras/stv1329

Document Version:
This is the Published Version.

Copyright and Reuse:
© 2015 The Authors Published by Oxford University Press on behalf of the Royal Astronomical Society.
Content in the UH Research Archive is made available for personal research, educational, or non-commercial purposes only. Unless otherwise stated all content is protected by copyright, and in the absence of an open licence permissions for further reuse of content should be sought from the publisher, author or other copyright holder.

Enquiries
If you believe this document infringes copyright, please contact the Research & Scholarly Communications Team at rsc@herts.ac.uk

Monthly Notices of the ROYAL ASTRONOMICAL SOCIETY

MNRAS **452,** 774–783 (2015) doi:10.1093/mnras/stv1329

The triggering of local AGN and their role in regulating star formation

Sugata Kaviraj,[1★] Stanislav S. Shabala,[2] Adam T. Deller[3] and Enno Middelberg[4]

[1]*Centre for Astrophysics Research, University of Hertfordshire, College Lane, Hatfield, Herts AL10 9AB, UK*
[2]*School of Mathematics and Physics, University of Tasmania, Private Bag 37, Hobart, TAS 7001, Australia*
[3]*The Netherlands Institute for Radio Astronomy (ASTRON), Postbus 2, NL-7990 AA Dwingeloo, the Netherlands*
[4]*Astronomisches Institut der Ruhr-Universität Bochum, Universitätsstraße 150, D-44801 Bochum, Germany*

Accepted 2015 June 5. Received 2015 June 1; in original form 2014 October 29

ABSTRACT

We explore the processes that trigger local AGN and the role of these AGN in regulating star formation, using ∼550 nearby galaxies observed by the mJy Imaging VLBA Exploration at 20 cm (mJIVE) survey. The $\gtrsim 10^7$ K brightness temperature required for an mJIVE detection cannot be achieved via star formation alone, allowing us to unambiguously detect nearby radio AGN and study their role in galaxy evolution. Radio AGN are an order of magnitude more common in early-type galaxies (ETGs) than in their late-type counterparts. The VLBI-detected ETGs in this study have a similar stellar mass distribution to their undetected counterparts, are typically not the central galaxies of clusters and exhibit merger fractions that are significantly higher than in the average ETG. This suggests that these radio AGN (which have VLBI luminosities $>10^{22}$ W Hz^{-1}) are primarily fuelled by mergers, and not by internal stellar mass-loss or cooling flows. Our radio AGN are a factor of ∼3 times more likely to reside in the UV–optical red sequence than the average ETG. Furthermore, typical AGN lifetimes (a few 10^7 yr) are much shorter than the transit times from blue cloud to red sequence (∼1.5 Gyr). This indicates that nearby (merger-triggered) AGN appear several dynamical time-scales into the associated star formation episode. This implies that such AGN typically couple only to residual gas, at a point where star formation has already declined significantly, and are, therefore, unlikely to play a significant role in regulating the star formation episode.

Key words: galaxies: elliptical and lenticular, cD – galaxies: evolution – galaxies: formation – galaxies: interactions.

1 INTRODUCTION

Understanding the assembly of massive galaxies, which dominate the stellar mass density in today's Universe (e.g. Kaviraj 2014a), is a fundamental topic in observational cosmology. While simple physics, implemented within the ΛCDM paradigm, successfully reproduces many observed properties of today's galaxies (e.g. Cole et al. 2000; Hatton et al. 2003; Springel, Di Matteo & Hernquist 2005a; Croton et al. 2006; Somerville et al. 2012), it has been recognized for some time that basic characteristics, such as the distribution of luminosities and colours, cannot be reproduced without invoking energetic feedback that quenches star formation at both ends of the galaxy mass function (Benson et al. 2003; Shabala & Alexander 2009).

In low-mass galaxies ($M_* \lesssim 10^{10}$ M$_\odot$; see Kaviraj et al. 2007d), typical energies imparted by supernovae (SNe) ejecta are sufficient to remove gas from the shallow potential wells and quench star formation. In the high-mass regime, however, the gravitational potential wells are too deep for SNe to be effective, and a more energetic source of feedback is required (e.g. Silk & Rees 1998). An attractive source of this feedback is the central black hole, because the potential energy released by the growth of the black hole is several orders of magnitude larger than the binding energy of the gas reservoir, even in the most massive galaxies (e.g. Fabian 2012).

Our theoretical picture of galaxy evolution postulates a key role for AGN in regulating star formation in massive galaxies across cosmic time. At high redshift, where most of today's stellar mass was assembled in intense star formation episodes, black holes were likely to be accreting close to the Eddington limit (Fabian 2012). Quasar-driven winds from such accretion episodes are postulated to remove gas reservoirs and truncate star formation after a few dynamical time-scales (e.g. Haehnelt, Natarajan & Rees 1998; Silk & Rees 1998; Fabian 1999; King 2003; Springel, Di Matteo & Hernquist 2005b; Fabian 2012). Notwithstanding this early removal of gas, a massive galaxy will retain the ability

★ E-mail: s.kaviraj@herts.ac.uk

© 2015 The Authors
Published by Oxford University Press on behalf of the Royal Astronomical Society

to accrete fresh gas, which may continue to fuel star formation. There are several potential sources of this late-stage accretion, such as mergers, stellar mass-loss (which feeds the internal hot gas reservoir) and cooling flows on to the central galaxies of clusters. The quiescence of massive galaxies must therefore be *maintained*, with the current theoretical consensus favouring feedback from AGN to perform this regulation over the latter half of cosmic time.

Observational work lends support to this theoretical picture. The peak of the cosmic star formation and black hole accretion rate densities coincide at $z \sim 2$ (e.g. Madau & Dickinson 2014), while in the local Universe galaxy (bulge) mass ($M_{\rm GAL}$) and black hole mass ($M_{\rm BH}$) show a strong correlation (see e.g. Magorrian et al. 1998; Ferrarese & Merritt 2000; Gebhardt et al. 2000; Häring & Rix 2004; Gültekin et al. 2009; McConnell et al. 2011), with $M_{\rm GAL} \sim M_{\rm BH} \times 1000$. Note that, while this correlation suggests coevolution between the two systems (e.g. Silk & Rees 1998; Granato et al. 2004; Springel et al. 2005b; Croton et al. 2006), it is possible that this scaling relation could be a natural consequence of hierarchical growth via galaxy merging, from initially uncorrelated distributions of black hole and stellar masses (e.g. Peng 2007; Jahnke & Macciò 2011).

In some individual galaxies, AGN-driven molecular outflows have been reported, both in the nearby Universe and at high redshift. While it is often difficult to attribute molecular outflows uniquely to the AGN as opposed to the starburst itself, the energetics of some outflows require the AGN to play a role, since the outflow rate far exceeds what can be driven by star formation alone (e.g. Nesvadba et al. 2008, 2011; Alexander et al. 2010; Rupke & Veilleux 2011; Sturm et al. 2011; Morganti et al. 2013; Nyland et al. 2013). Perhaps the strongest evidence for AGN feedback comes from the central galaxies of clusters, which are surrounded by hot gas with short cooling times (Fabian 1994). Unless the initial mass function is dominated by low-mass stars (e.g. Cappellari et al. 2012), as could be possible in the high-pressure environment of a cluster centre (Fabian, Nulsen & Canizares 1982), the derived star formation rates (SFRs) in these systems appear to be several orders of magnitudes lower than the mass deposition rates expected from cooling. This suggests that the high temperature of the gas is being maintained, a plausible heat source being the central black hole (e.g. Tabor & Binney 1993; McNamara & Nulsen 2007; Cattaneo et al. 2009; Fabian 2012).

While individual examples of the interaction of AGN with their host galaxies are being found, an understanding of the *global* role of black holes in regulating star formation requires an analysis of survey-scale samples of AGN. Recent work using optical emission-line AGN, drawn from the Sloan Digital Sky Survey (SDSS; Abazajian et al. 2009), has demonstrated a coincidence of rising AGN activity and declining SFRs, with the peak of the optical AGN activity appearing to lag behind the peak of the star formation by a few hundred Myr. This time lag is observed across the full spectrum of star formation activity, from the strongly star forming luminous infrared galaxies (Kaviraj 2009) to the more weakly star forming early-type galaxies (ETGs; Schawinski et al. 2007; Wild, Heckman & Charlot 2010; Shabala et al. 2012). As we explore in our analysis below, a time delay in the onset of the AGN has important implications for its ability to regulate star formation, since the gas reservoir may have been significantly depleted before the AGN has a chance to couple to it.

A drawback of past survey-scale studies is that most data sets are not able to unambiguously determine the presence of a radio AGN, which drives the putative maintenance mode feedback. While surveys like the SDSS can identify optical emission-line AGN, optical and radio AGN often show little correlation (Best et al. 2005), making it difficult to establish the presence of the radio mode using emission lines alone. Furthermore, radio surveys like FIRST and NVSS typically do not resolve the galaxy core, making it difficult to ascertain how much of the radio emission is driven by star formation and how much of it is attributable to a radio AGN.

Unlike the methods discussed above, very long baseline interferometry (VLBI) in the radio wavelengths can unambiguously identify AGN, because the high resolution requires brightness temperatures of $\sim 10^6$ K for a detection. Such conditions cannot be achieved via star formation alone and require non-thermal sources, such as supernova remnants (SNRs), radio SNe or AGN. However, only in the very local Universe, and in rather extreme cases like Arp 220 (Lonsdale et al. 2006), can clusters of luminous SNRs or SNe be sufficiently bright for a VLBI detection. In the case of this particular study, the galaxies that will underpin our analysis are early-type systems which have significantly lower SFRs than Arp 220, which has an SFR of several hundred solar masses per year (e.g. Iwasawa et al. 2005; Baan 2007). They also lie much further away than Arp 220 (see Fig. 3), which has a redshift of 0.018. The compact (parsec-scale) radio emission in these systems is, therefore, inconsistent with originating from star formation.

The power of VLBI, then, lies in its ability to make unambiguous identification of AGN activity. The identification of AGN in lower resolution radio surveys typically requires detection of excess radio flux over what is expected from star formation (biasing samples towards AGN that dominate the star formation), or a dense gas environment against which the AGN does work and produces detectable radio lobes (possibly introducing a bias towards AGN in large groups and clusters). In contrast, VLBI is able to identify AGN irrespective of the properties of the host galaxy (e.g. stellar mass and local environment) or the level of star formation in the system, making it an ideal tool for an exploration of local AGN and their role in regulating star formation in the nearby Universe. However, this certainty comes with some limitations; of the total radio emission generated by AGN activity, only a fraction will typically be confined to the parsec-scale core/jet at the site of the central black hole, as extended radio lobes will often be present. The prominence of the compact core depends on the source age and orientation (which can result in Doppler boosting or deboosting of the compact emission). Finally, hotspots at the site of the jet interaction with the interstellar medium – e.g. compact symmetric objects, which are very young radio sources with similar structures as classical sources but on scales several magnitudes smaller – will also be visible in VLBI observations, meaning that although VLBI detections can unambiguously be associated with AGN, they cannot in every case be associated with AGN *cores*. However, this last case can usually be distinguished on the basis of morphology.

The plan for this paper is as follows. In Section 2, we describe the various data sets that underpin our study. In Section 3, we explore the processes that trigger the AGN in our galaxy sample. In Section 4, we study the point in star formation episodes at which radio AGN typically appear, and explore the implications for the regulation of local star formation via AGN feedback. We summarize our findings in Section 5. Throughout, we employ the *WMAP*7 cosmological parameters (Komatsu et al. 2011) and photometry in the AB system (Oke & Gunn 1983).

2 DATA

2.1 Radio VLBI data

The mJy Imaging VLBA Exploration at 20 cm (mJIVE; hereafter) is using the VLBA to systematically observe objects detected by the Faint Images of the Radio Sky at Twenty cm (FIRST) survey (Deller & Middelberg 2014). mJIVE utilizes short segments scheduled in bad weather or with a reduced number of antennas during which no highly rated science projects can be scheduled. After 18 months of observing, the mJIVE survey has imaged more than 25 000 FIRST sources, with more than 5000 VLBI detections. While the sensitivity and resolution varies between mJIVE fields, the median detection threshold of 1.2 mJy beam^{-1} and typical beam size of 6×17 mas correspond to a detection sensitivity of $\sim 10^7$ K, with a typical variation between fields of around a factor of 2. We refer readers to Deller & Middelberg (2014) for further details of the survey.

2.2 SDSS and *GALEX* photometry

The mJIVE targets are cross-matched with the latest versions of the SDSS and *GALEX* surveys (Martin et al. 2005; Morrissey et al. 2007). SDSS provides five-band (*ugriz*) optical photometry, while *GALEX* provides ultraviolet (UV) photometry in two passbands shortward of 3000 Å. For the purposes of this work, we only use the *GALEX* near-ultraviolet (NUV) filter, which is centred at 2300 Å. Following Shabala et al. (2008), we use a matching radius of 2 arcsec for the radio-optical matching, which yields high (96 per cent) completeness and low (0.3 per cent) contamination. *GALEX* observations are then matched to the SDSS objects with a matching radius of 4 arcsec (see e.g. Kaviraj et al. 2007a). Magnitudes are corrected for Galactic extinction using Schlegel, Finkbeiner & Davis (1998) and *K*-corrected using the public KCORRECT code of Blanton & Roweis (2007).

2.3 Stellar masses and optical AGN diagnostics

In our analysis below, we employ published stellar masses and emission-line diagnostics from the latest version of the publicly available MPA-JHU value-added SDSS catalogue (Kauffmann et al. 2003; Brinchmann et al. 2004; Tremonti et al. 2004).[1] The emission-line class of the galaxy is derived via a standard line-ratio analysis (Kauffmann et al. 2003, see also Baldwin, Phillips & Terlevich 1981; Veilleux & Osterbrock 1987; Kewley et al. 2006), using the values of [N II]/H α and [O III]/H β measured from the SDSS spectra of individual galaxies. Objects in which all four emission lines are detected with a signal-to-noise ratio greater than 3 are classified as either 'star forming', 'composite', 'Seyfert' or 'LINER', depending on their location in the [N II]/H α versus [O III]/H β diagram. Galaxies which do not have a detection in all four lines are classified as 'quiescent' (Kauffmann et al. 2003). We refer readers to Brinchmann et al. (2004) and Tremonti et al. (2004) for full details of the modelling.

2.4 Local environment

We study the local environments of our galaxies by using the group catalogue of Yang et al. (2007), who use a halo-based group finder to separate the SDSS into over 300 000 structures with a broad dynamic range, from rich clusters to isolated galaxies. This catalogue provides estimates of the masses of the host dark matter (DM) haloes of individual SDSS galaxies, which are related to the traditional classifications of environment ('field', 'group' and 'cluster'). Cluster-sized haloes typically have masses greater than 10^{14} M$_\odot$, while group-sized haloes have masses between 10^{13} and 10^{14} M$_\odot$. Smaller DM haloes constitute what is commonly termed the field (e.g. Binney & Tremaine 1987).

2.5 Recent star formation histories

We estimate parameters governing the recent star formation history (SFH) of individual galaxies by comparing their *GALEX*/SDSS (NUV, *u*, *g*, *r*, *i*, *z*) photometry to a library of synthetic photometry, generated using a large collection of model SFHs. Since VLBI detections are overwhelmingly found in ETGs (see Section 2.7 below), our SFHs are tailored to these systems. Given that the bulk of the stellar mass in ETGs forms rapidly at high redshift (e.g. Trager et al. 2000), we model the underlying stellar population using an instantaneous burst at high redshift that takes places at $z = 3$. The recent star formation episode is modelled using a second instantaneous burst, which is allowed to vary in age between 0.001 Gyr and look-back time corresponding to $z = 3$ in the rest-frame of the galaxy, and in mass fraction between 0 and 1. Our parametrization is similar to previous work that has quantified early-type SFHs using UV/optical data (e.g. Jeong et al. 2007, Kaviraj et al. 2007a).

To build the library of synthetic photometry, each model SFH is combined with a metallicity in the range 0.1–2.5 Z$_\odot$ and a value of dust extinction parametrized by $E_{\rm B-V}$ in the range 0–0.5, via the empirical dust prescription of Calzetti et al. (2000). Photometric predictions are generated by combining each model SFH with the chosen metallicity and $E_{\rm B-V}$ values and convolving with the stellar models of Yi (2003) through the *GALEX* and SDSS filtercurves. Since our galaxy sample spans a range of redshifts, equivalent libraries are constructed at redshift intervals of $\delta z = 0.02$.

Values of the free parameters are estimated by comparing each galaxy to every model in the synthetic library and calculating the model likelihoods ($\exp - \chi^2/2$, e.g. Sivia 1996). From the joint probability distribution, each parameter is marginalized to extract its one-dimensional probability density function (PDF). The median of this PDF is taken to be the best estimate of the parameter in question and the 16 and 84 percentile values are used to calculate an associated 'one-sigma' uncertainty. In the analysis that follows, we explore the median values of the age of the recent starburst (t_2). The typical uncertainties in this parameter are better than 15 per cent i.e. the uncertainty in $\log(t2)$ is around 0.05 dex or less. Note that accurate parameter estimation requires the inclusion of UV photometry (see e.g. Kaviraj et al. 2007c), so this SFH analysis is only performed for galaxies that have *GALEX* detections.

2.6 Visually classified galaxy morphologies

We use direct visual inspection of SDSS colour images to classify our galaxies into two broad morphological types: early-type galaxies (ETGs) and late-type galaxies (LTGs). While classification into fine morphological classes (e.g. ellipticals, S0, Sa, etc.) is difficult to achieve beyond $z \sim 0.2$ using SDSS images (see e.g. Kaviraj 2009), splitting our galaxies into such broad morphological classes is robust to $z \sim 0.3$, as indicated by Figs 1 and 2 which show typical examples of ETGs and LTGs across the redshift range studied in this paper.

[1] http://www.mpa-garching.mpg.de/SDSS/DR7/

Figure 1. Example SDSS images of early-type mJIVE targets. The galaxies in the top row are in the redshift range $z < 0.1$, those in the middle row are in the redshift range $0.1 < z < 0.2$ and those in the bottom row are in the redshift range $0.2 < z < 0.3$.

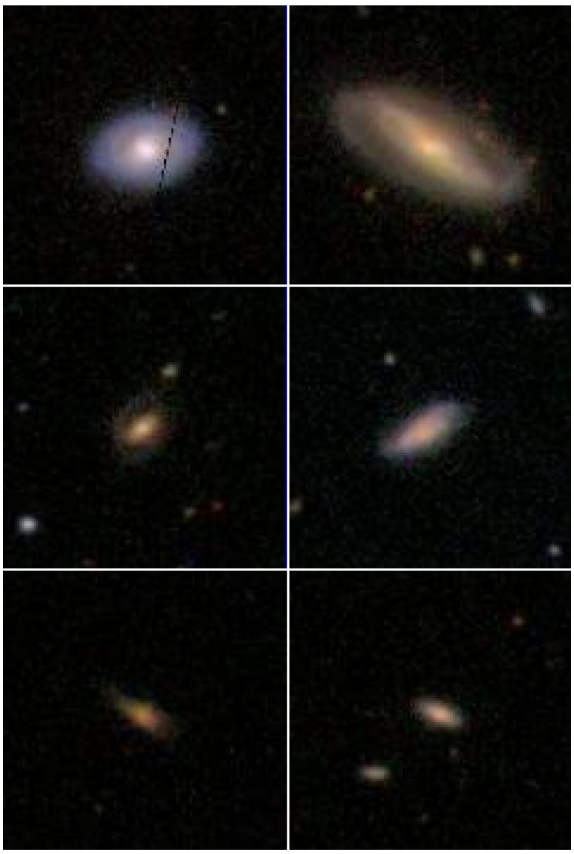

Figure 2. Example SDSS images of late-type mJIVE targets. The galaxies in the top row are in the redshift range $z < 0.1$, those in the middle row are in the redshift range $0.1 < z < 0.2$ and those in the bottom row are in the redshift range $0.2 < z < 0.3$.

2.7 The final galaxy sample and basic properties

The final galaxy sample that underpins this study comprises 546 mJIVE targets which have stellar masses and SFRs from the MPA-JHU catalogue, environments from the Yang et al. group catalogue, SFHs derived via spectral energy distribution (SED) fitting and visually classified morphologies. ETGs and LTGs comprise 76 per cent (415 galaxies) and 24 per cent (131 galaxies) of the mJIVE targets, respectively. *GALEX* coverage is available for around two thirds of the sample, so parts of our subsequent analysis that rely on *GALEX* data are restricted to a somewhat smaller fraction of objects.

We find that the VLBI detection rate in mJIVE targets that are ETGs is ∼30 per cent, while the corresponding rate in LTGs is ∼3 per cent. However, since black hole mass scales with galaxy stellar mass (e.g. McConnell et al. 2011) and ETGs are on average more massive than LTGs, a fairer comparison can be made by comparing the LTG detection rate to a subsample of ETGs that have the same stellar mass and redshift distribution as the LTGs. The detection rate in this matched ETG subsample is ∼26 per cent. Note that the distributions of FIRST fluxes of the LTGs and the ETG subsample are very similar, making these values a reasonable estimate of the relative detection rate in the two morphological classes. Radio AGN are, therefore, almost an order of magnitude more frequent in ETGs than in their LTG counterparts, in agreement with the past literature (e.g. Ledlow et al. 2001). The VLBI-detected LTGs will be the subject of a forthcoming paper (Kaviraj et al. 2015). Given the dearth of radio AGN in the LTGs, our subsequent analysis focuses only on the ETG population.

Since the mJIVE targets are, by construction, all detected by FIRST, it is useful to define a 'control' sample of ETGs that are not FIRST-detected and to which we will compare the ETG VLBI detections at various points in our analysis below. This control sample is selected via the Galaxy Zoo project (Lintott et al. 2008), which has used 500 000+ volunteers from the general public to produce accurate morphological classifications for the entire SDSS via visual inspection of SDSS colour images. The galaxies in our ETG control sample have a Galaxy Zoo 'early-type' probability of more than 90 per cent and are selected to have the same redshift, stellar mass and environment distribution as the ETGs with VLBI detections.

Before we begin our analysis, we briefly explore the typical AGN luminosities being sampled here and whether AGN detectability varies across our redshift range of interest (possibly leading to selection effects that might affect our analysis). The left-hand panel of Fig. 3 presents the radio luminosities of the AGN in our sample. The black histogram indicates the radio luminosities of our VLBI-detected systems, while the orange histogram shows upper limits in galaxies that are not detected by mJIVE. The median radio luminosity of the VLBI detections is around $10^{23.5}$ W Hz^{-1}, while the lowest luminosities are around 10^{22} W Hz^{-1} – the AGN studied here are, therefore, typically brighter than this latter value. The right-hand panel of this figure shows that the VLBI detections and non-detections have similar redshift distributions. A

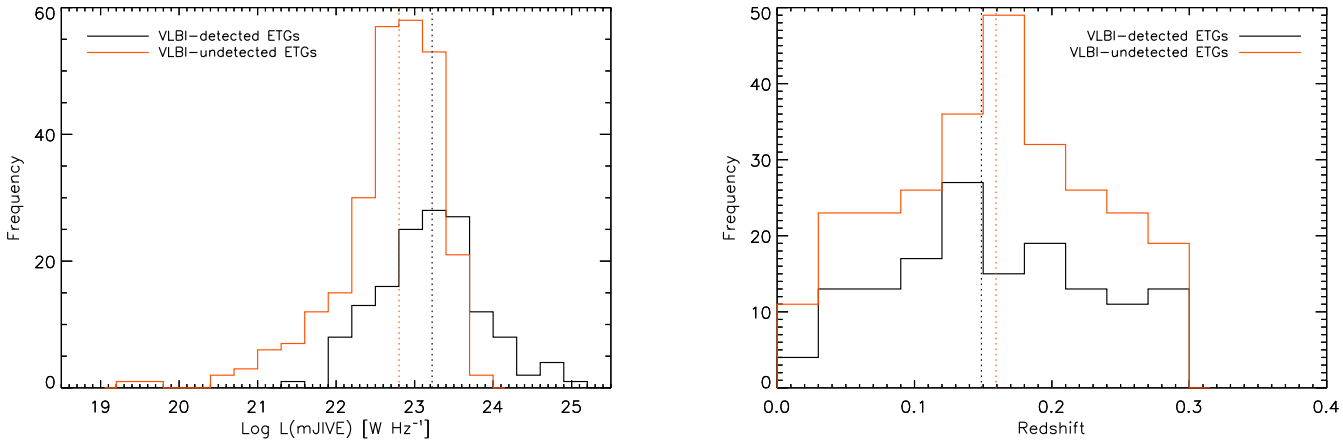

Figure 3. Left: mJIVE luminosities of VLBI detections (black) and upper limits in the VLBI non-detections (orange). Right: the redshift distribution of the VLBI detections (black) and their undetected counterparts (orange). Vertical dotted lines indicate median values.

Kolmogorov–Smirnov (KS) test yields a p-value of 0.64, indicating that the two redshift samples are highly likely to be drawn from the same parent distribution. The similarity in the redshift distributions indicates that the detectability of our AGN in VLBI does not vary in the redshift range studied here ($z < 0.3$).

3 TRIGGERING OF LOCAL AGN

We begin by exploring the processes that are likely to be fuelling the radio AGN in our sample. There are several sources of gas that may trigger AGN, such as internal stellar mass-loss (which feeds the internal hot gas reservoir), cluster-scale cooling flows (which will operate in the central galaxies of clusters) and mergers. Fig. 4 shows that the stellar mass distribution of the VLBI detections is similar to that of their undetected counterparts. A KS test between the two samples yields a p-value of 0.23, indicating that they are likely to be drawn from the same parent distribution. This similarity suggests that the AGN are unlikely to be triggered by internal stellar mass-loss, since more massive galaxies will produce larger gas reservoirs via this process and one might expect the host galaxies of our VLBI detections to then be preferentially more massive.

Further insight into the gas supply can be gained by studying the local environments of our AGN. The top panel of Fig. 5 indicates that the VLBI detections in this study preferentially lie outside clusters (i.e. in relatively low-density environments). In addition, those that do inhabit clusters are not central galaxies but are typically found at reasonably large group-centric radii (bottom panel of Fig. 5). The vast majority of radio AGN in this particular sample are, therefore, unlikely to be fuelled by cluster-scale cooling flows.

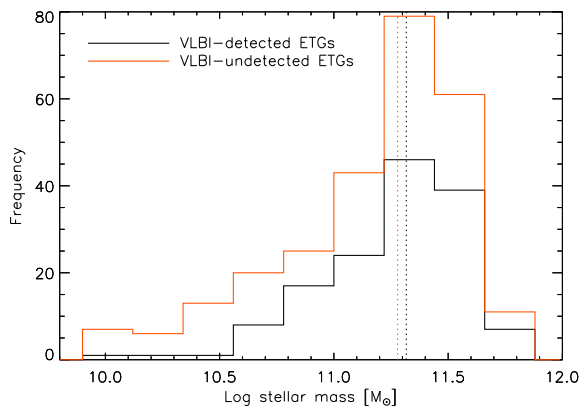

Figure 4. The stellar mass distribution of VLBI-detected (black) and undetected (orange) ETGs in our sample. Vertical dotted lines indicate median values.

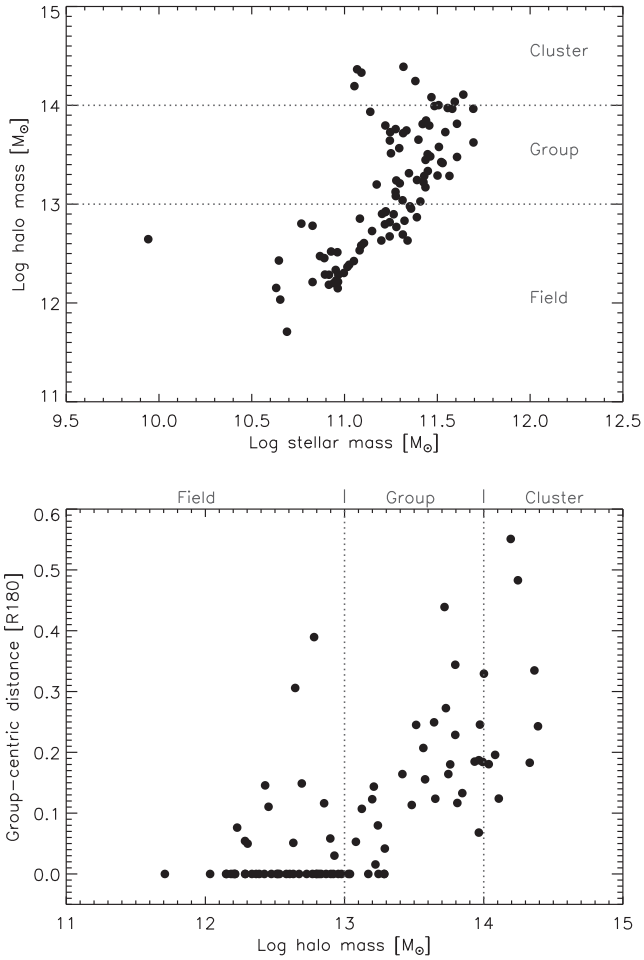

Figure 5. DM halo versus stellar mass (top) and group-centric radius versus halo mass (bottom) for ETGs in our sample. The Yang et al. (2007) group catalogue define DM haloes as having an overdensity of 180. The group-centric radii are, therefore, calculated by dividing the distance of the galaxy in question by R_{180}.

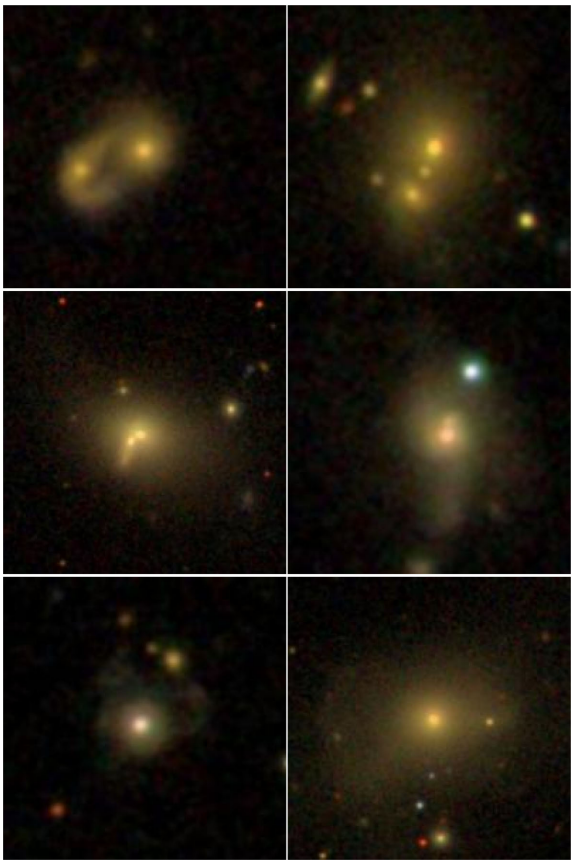

Figure 6. Examples of VLBI-detected ETGs in mergers. The top two rows indicate systems that are ongoing mergers, while the bottom row indicates systems that are post-mergers.

While the arguments above point towards mergers being an important trigger for our radio AGN, we quantify this by visually inspecting our VLBI detections and flagging systems that are either ongoing mergers (two interacting cores with tidal bridges between them, see top and middle rows of Fig. 6) or post-mergers (one nucleus with tidal debris around it, see bottom row of Fig. 6). We note that a drawback of the standard depth (51 s) SDSS images is that faint tidal features, such as those produced by relatively gas-poor or low-mass-ratio mergers, can be difficult to detect in the images (e.g. Kaviraj 2010). Hence, the merger fraction calculated here is strictly a lower limit. Therefore, in addition to identifying ongoing and post-mergers via visual inspection, we also search for neighbouring objects around each galaxy that are within a projected separation of 30 kpc, with either spectroscopic redshifts with a maximum velocity differential of 500 km s^{-1} or photometric redshifts that are, within their uncertainties, consistent with the galaxy in question. We restrict these photometric neighbours to objects that have accurate photometric redshifts (uncertainties less than 20 per cent). The 30 kpc separation employed is motivated by work which shows that star formation and AGN activity can be efficiently triggered when the separation between interacting galaxies is within 30 kpc (see e.g. Patton et al. 2002; Scudder et al. 2012; Scott & Kaviraj 2014). To quantify the role of merging in triggering our radio AGN, we perform an identical exercise (visual inspection + neighbours analysis) on our control sample of ETGs.

Table 1 presents the merger fractions for the VLBI-detected ETGs and their control counterparts, split by environment. We provide merger fractions with and without the neighbour analysis (shown in brackets). Note that the visually classified merger fractions in the control sample are consistent with the findings of past work which has calculated merger fractions in massive galaxies via visual inspection of SDSS images (Darg et al. 2010a,b). The bottom row in this table indicates the enhancement of the merger fraction in the AGN population compared to their control counterparts. We find that the merger fractions in the AGN population are several factors higher than that in the general galaxy population, irrespective of the local environment of the systems. These results are generally consistent with the broader literature, in which a coincidence of AGN and merger activity (at various stages of the merger process) has been reported (e.g. Inskip et al. 2010; Koss et al. 2010; Schawinski et al. 2010; Ellison et al. 2011; Carpineti et al. 2012). In particular, Pace & Salim (2014) have recently studied the local neigbourhood of radio-loud galaxies in the nearby Universe, finding a clear excess of satellites within 100 kpc, compared to their radio-quiet satellites. Recalling that our merger fractions are strictly lower limits, it appears reasonable to conclude that an important trigger for the radio AGN in our sample is galaxy merging.

Table 1. Merger fractions for radio AGN and for a control sample of ETGs, split by environment. The last row indicates the relative enhancement in the merger fraction in AGN compared to the general ETG population. The values in brackets include the neighbour analysis, while those without brackets only include systems that are flagged as ongoing or post-mergers via visual inspection (see the text in Section 3 for details).

	Field	Groups and clusters
AGN	$0.36^{\pm0.03}$ ($0.45^{\pm0.04}$)	$0.28^{\pm0.07}$ ($0.33^{\pm0.07}$)
Control	$0.11^{\pm0.02}$ ($0.14^{\pm0.02}$)	$0.06^{\pm0.01}$ ($0.08^{\pm0.01}$)
f(AGN)/f(Control)	3.3 (3.2)	4.7 (4.1)

We note that, given these high merger fractions and the fact that our VLBI detections are not central galaxies of clusters, our subsequent analysis may largely probe 'cold-mode' AGN, which are fuelled via accretion from a cold gas disc fed by mergers and interactions (e.g. Hardcastle, Evans & Croston 2007; Best & Heckman 2012; Shabala et al. 2012), rather than 'hot-mode' AGN, which are fuelled via direct cooling of hot gas. It is difficult to quantify the relative proportion of AGN in either fuelling mode because the shallow SDSS images inevitably lead to an underestimate of the merger fractions and therefore a corresponding underestimate of the fraction of cold-mode systems.

4 TIME DELAY IN THE ONSET OF AGN AND IMPLICATIONS FOR REGULATION OF STAR FORMATION

We proceed by exploring the point in the evolution of star formation episodes when radio AGN typically appear, which has important implications for the potential impact of AGN feedback on star formation. For feedback to be most effective, the AGN must appear promptly after the onset of star formation (or at least before the star formation peaks), when the systems are gas rich. However, if the onset of the AGN takes place several dynamical time-scales into the starburst, then a large fraction of the gas reservoir will have been depleted before the AGN has a chance to interact with it, reducing its role in regulating star formation. It is worth noting here that the ETGs in our study (see Fig. 7) are in the luminosity range

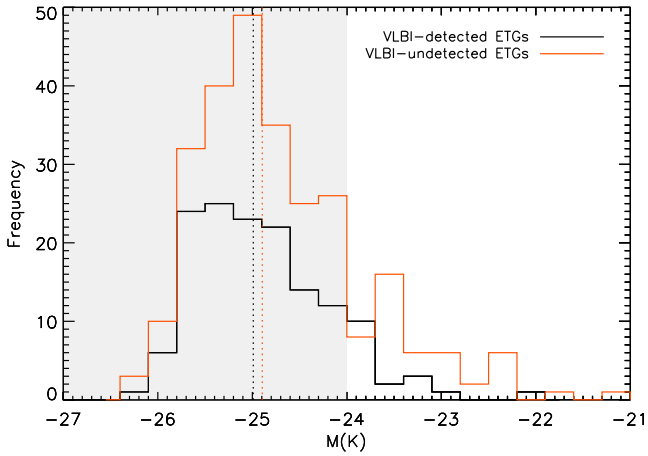

Figure 7. Absolute *K*-band luminosity distribution of the ETGs in our sample. The shaded region indicates the luminosity range in which AGN feedback is expected to play an important role in regulating star formation (e.g. Benson et al. 2003). Vertical dotted lines indicate median values.

where AGN feedback is expected to play a key role in regulating and quenching star formation (e.g. Benson et al. 2003).

Fig. 8 shows that the VLBI-detected ETGs primarily reside on the UV–optical red sequence. We restrict this analysis to $z < 0.12$ (135 galaxies), because the *GALEX* UV red-sequence detection rate is ∼95 per cent in this redshift range but drops rapidly thereafter (see fig. 1 in Kaviraj et al. 2007a). Note that the *GALEX*-detected ETGs at $z < 0.12$ are representative of the low-redshift ETG population as a whole – the only unique quality of this subsample is its completeness, due to the high detection rate of red-sequence objects. Thus, the results derived from this subset of ETGs holds generally.

The high sensitivity of the UV wavelengths to star formation means that even small mass fractions of young stars (of the order of a percent or less) will drive ETGs into the UV–optical blue cloud

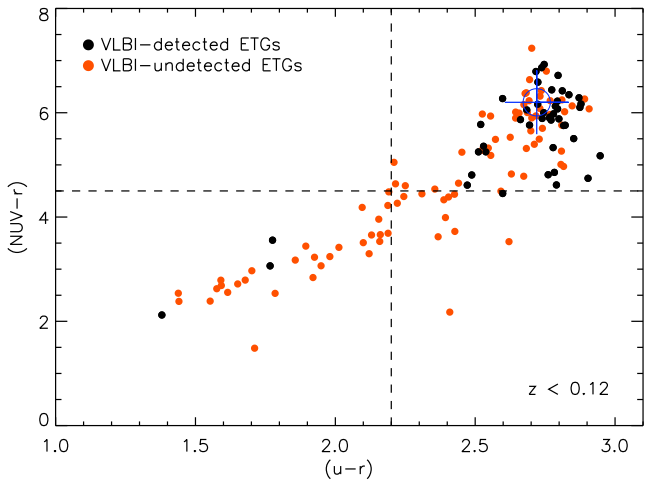

Figure 8. UV–optical colours of ETGs in our sample. The VLBI-detected ETGs are shown in black, while ETGs that are undetected are shown in orange. The median colour of the general ETG population, from the SDSS control sample of ETGs, is shown using the blue crosshair. The dashed lines demarcate the blue cloud (bottom left region) and red sequence (everything else), as indicated by the literature (see e.g. Strateva et al. 2001; Wyder et al. 2007). Note that this analysis is restricted to $z < 0.12$ (135 galaxies), where the *GALEX* UV red-sequence detection rate is ∼95 per cent.

Table 2. Ratio of blue cloud to red-sequence objects in our ETGs. Only ETGs at $z < 0.12$ are considered here because the UV red-sequence detection rate is ∼95 per cent in this redshift range but drops rapidly thereafter.

	Blue-to-red ratio
VLBI-detected ETGs	$0.09^{\pm 0.04}$
Control sample ETGs	$0.25^{\pm 0.06}$
VLBI-undetected ETGs	$0.80^{\pm 0.15}$

(e.g. Yi et al. 2005, Kaviraj et al. 2007a), making the UV–optical colour space the most effective route to separating star-forming systems from their more quiescent counterparts. Fig. 8 therefore suggests that radio AGN typically inhabit galaxies in which star formation activity is low i.e. has declined significantly since the onset of the starburst. Table 2 presents the blue-cloud to red-sequence ratios for the VLBI-detected ETGs and the control sample, where galaxies that have $(\mathrm{NUV} - r) < 4.5$ are classified as 'blue' and those with $(\mathrm{NUV} - r) > 4.5$ are classified as 'red' (Wyder et al. 2007). The blue-to-red ratios in the VLBI-detected ETGs and the control sample are 9 and 25 per cent, respectively (the VLBI-undetected ETGs show a ratio of 80 per cent). The likelihood of finding VLBI detections in the blue cloud is, therefore, around a factor of 3 lower than in the general ETG population.

If AGN were triggered promptly after the onset of star formation, one would expect the blue-to-red ratio in the VLBI detections to be higher than that in the general ETG population (the opposite to what is observed). It is worth exploring whether our red-sequence AGN could originally have been triggered promptly while their host galaxies were in the blue cloud and have remained active as their host galaxies transited across the colour–colour diagram. This is possible if AGN lifetimes are comparable to the time it takes for a galaxy to transit from the blue cloud to the red sequence. The typical lifetimes of AGN (i.e. the lifetime of the 'on' phase), in galaxies within our mass range of interest, are a few 10^7 yr (e.g. Shabala et al. 2008, see their fig. 13). We can estimate a lower limit on blue-to-red transit times, via past work on nearby post-starburst (E+A) galaxies. E+A galaxies are systems that do not show emission lines that trace ongoing star formation (e.g. H α) but exhibit deep Balmer absorption lines that are indicative of significant recent star formation. These galaxies have, therefore, experienced a recent starburst which has been truncated. Kaviraj et al. (2007b) have shown that the median blue-to-red transit time of E+A galaxies in the nearby Universe is ∼1.5 Gyr (see their Fig. 7), consistent with theoretical work on the likely time-scales for this transit (e.g. Kaviraj et al. 2011b). Since star formation has been completely quenched in these systems, E+A galaxies will transit from blue cloud to red sequence in the *shortest* possible time.

Given that typical AGN lifetimes are much shorter than ∼1.5 Gyr, the radio AGN that are observed on the UV–optical red sequence are unlikely to have appeared in their host galaxies when these systems were originally in the blue cloud. Even if the observed AGN are the result of retriggering on time-scales of around a Gyr (e.g. Enßlin & Gopal-Krishna 2001), the paucity of AGN in the blue cloud and the arguments above indicate that the AGN episodes that directly follow the onset of starbursts in ETGs are unlikely to be prompt.

It is instructive to estimate the magnitude of the time delay between the onset of star formation and the onset of the AGN, by comparing the age of the starburst (estimated in Section 2.4 via SED fitting) to the dynamical time-scale (τ_{dyn}) in individual

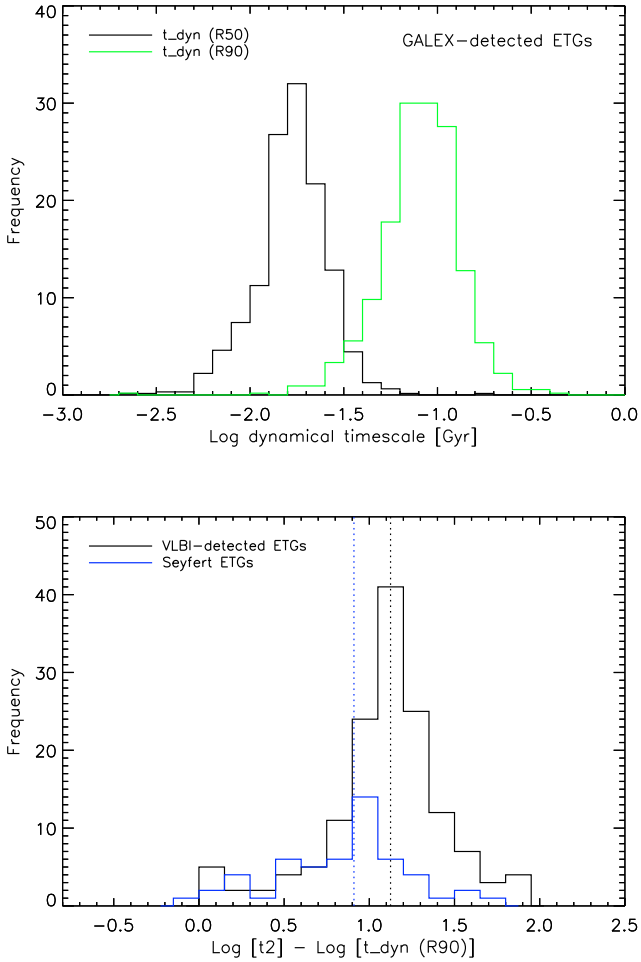

Figure 9. TOP: dynamical time-scales of the ETGs in our sample, calculated both using radii that contain 50 per cent (R_{50}; black histogram) and 90 per cent (R_{90}; blue histogram) of the r-band Petrosian flux as the value for R in equation (1). BOTTOM: the ratio of the age of the starburst and the dynamical time-scale in VLBI-detected (black histogram) and Seyfert (blue histogram) ETGs. Vertical dotted lines indicate median values.

galaxies, defined as[2]

$$\tau_{\rm dyn} = \left(\frac{2R^3}{GM}\right)^{1/2}. \quad (1)$$

In the top panel of Fig. 9, we present the $\tau_{\rm dyn}$ values of our ETGs, calculated both using radii that contain 50 per cent (R_{50}; black histogram) and 90 per cent (R_{90}; blue histogram) of the r-band Petrosian flux as the value for R in equation (1). While our $\tau_{\rm dyn}$ values have been calculated using the stellar properties of the galaxies in question, our values using R_{90} are very similar to the star formation time-scales of gas discs in local ETGs, calculated via CO measurements (0.05–0.2 Gyr; Young 2002). In the bottom panel of Fig. 9, we present the ratio of the age of starburst to the dynamical time-scale in our VLBI detections (calculated using R_{90}). Dividing the starburst age by the dynamical time-scale provides a normalized quantity, enabling a fairer comparison of galaxies that have different radii and masses (recall that the typical uncertainties in the age of the starburst are better than 0.05 dex). We find that the ages of the star formation episodes in our VLBI detections are typically several multiples of the dynamical time-scales of the galaxies in question, suggesting that these radio AGN are triggered relatively late into the associated starbursts (note that the figure indicates that this is also true of Seyferts ETGs, in line with the findings of the recent literature). In such a scenario, the ability of the AGN to regulate star formation will be reduced, since a significant fraction of the gas reservoir is likely to have been depleted before the AGN switches on. While the AGN may well couple to the remaining gas reservoir and drive an outflow, the overall impact of such feedback episodes will be to mop up residual gas at a point where star formation has already declined.

Our results are consistent with recent observational and theoretical work which suggests that there is a time delay between the onset of star formation episodes and the onset of the associated AGN activity in the nearby Universe. As noted in the introduction, a number of studies have shown that the peak of optically identified AGN activity is delayed compared to the onset of star formation by several hundred Myr. This is found to be the case across the full spectrum of star formation activity, from strongly star forming systems such as luminous infrared galaxies (Kaviraj 2009) to the more weakly star forming ETGs (e.g. Davies et al. 2007; Schawinski et al. 2007; Wild et al. 2010; Shabala et al. 2012; Yesuf et al. 2014).

Some physical explanations have been proposed in the recent literature to explain this observed time lag. Supernova feedback during the peak phase of star formation activity may disrupt the supply of gas on to the black hole, with preferential fuelling in the post-starburst phase from stellar mass-loss (Wild et al. 2010). It remains unclear if fuelling purely via stellar mass-loss is appropriate for systems that are likely to be accreting material in the cold phase (e.g. Lonsdale et al. 2003; Kondratko et al. 2006; Nenkova et al. 2008). The cause of this delay could also be dynamical in nature. During the peak of the starburst, when the system is rich in gas, most regions are unstable and more conducive to star formation, making this the favoured mode of gas consumption (Cen 2012). Inflow on to the black hole requires further removal of angular momentum, which becomes efficient only after most of the gas has been consumed by star formation activity (Hopkins 2012), introducing a time lag between the onset of star formation and the triggering of the AGN. Realistic hydro-dynamical models appear to naturally produce a time lag that is qualitatively similar to what is observed in nearby ETGs (Hopkins 2012, see also Cox et al. 2006, Robertson et al. 2006).

It should be noted that our results do not imply that AGN feedback does not take place at all in the nearby Universe. As mentioned in the introduction, strong evidence exists for the regulation of star formation in central cluster galaxies via AGN-driven heating of cooling flows. However, while the AGN appears to couple efficiently to gas that is acquired via cooling, the onset of the AGN appears to be significantly delayed when the gas is brought in via mergers. This time lag implies that the impact of AGN on star formation driven by mergers is relatively limited, because they are triggered at a point in the star formation episode when the gas reservoir has already been significantly depleted.

The results of this study are strongly aligned with work on star formation in ETGs. The recent literature that leverages data in the UV wavelengths has demonstrated that, contrary to our classical notion of ETGs being passively evolving galaxies, widespread star formation exists in these galaxies (e.g. Yi et al. 2005; Jeong et al. 2007; Kaviraj et al. 2007 a). A strong correspondence is observed between blue UV colours and morphological disturbances, indicating that the star formation in merger driven. However, the major

[2] Using the equation of motion $s = \frac{1}{2}at^2$, the dynamical time-scale follows by setting $a = g = (GM/R^2)$ and $s = R$, where M and R are the mass and radius of the system, respectively.

merger rate is too low to reproduce the fraction of disturbed ETGs, implying that minor mergers drive the stellar mass growth in these systems (Kaviraj et al. 2009, 2011a), with a significant minority (20–30 per cent) of the stellar mass forming after $z \sim 1$ (Kaviraj et al. 2008; see also Kaviraj 2014b). Based on our findings here, it is likely that the merger-driven star formation that is observed in nearby ETGs is possible precisely because the associated AGN activity is triggered late into these star formation episodes and cannot strongly regulate or quench the starburst. The weak coupling of AGN to merger-driven star formation therefore makes this the dominant mode of stellar mass growth in nearby ETGs.

What do our results imply for our general paradigm of AGN-regulated galaxy growth? Two issues are worth noting here. First (as mentioned above), since our sample is drawn from the general galaxy population, it is not dominated by central cluster galaxies and does not offer constraints on the role of AGN in such environments. The past literature, however, provides compelling evidence for feedback in such environments, through AGN heating of cooling flows. In the nearby Universe, strong AGN feedback is therefore likely to be most efficient in (and largely restricted to) these environments. Secondly, since the galaxies studied here are local, our results do not offer insight into the interaction of AGN with their host galaxies at high redshift. Given that the cosmic star formation and black hole accretion rates peak at $z \sim 2$, it is around these redshifts that the bulk of today's stellar mass formed. This is also the epoch at which the observed scaling relations – such as the $M_{\rm BH}$–σ correlation – were established, most likely over short time-scales (<1 Gyr), as indicated by the high [α/Fe] ratios in massive ETGs (e.g. Trager et al. 2000; Thomas et al. 2005).

For this high-redshift scenario to be strongly influenced by AGN feedback, the situation must be different at high redshift. In particular, AGN must be triggered in 'normal' (i.e. non-merging) LTGs, which dominate the star formation budget at these epochs (e.g. Kaviraj et al. 2013) and couple efficiently to their host galaxies in order to produce the scaling relations over short time-scales. The latter requires prompt triggering of the AGN, presumably leading to a smaller (or negligible) colour offsets between the star forming and AGN populations at these epochs. While the scope of this study does not allow us to probe these issues (since our sample is local), in forthcoming work we will study the coevolution of AGN and their host galaxies at higher redshift, and present preliminary evidence that the requirements mentioned above are indeed satisfied by the radio AGN population around the epoch of peak cosmic star formation.

5 SUMMARY

We have studied ∼350 massive, nearby galaxies, observed by the mJIVE survey, to explore the role of AGN in regulating star formation in nearby galaxies. The $\gtrsim 10^7$ K temperatures required for an mJIVE detection cannot be achieved via star formation alone, allowing us to unambiguously detect radio AGN and study their role in galaxy evolution in the nearby Universe.

VLBI detections are overwhelmingly found in ETGs, with the detection rate in LTGs being an order of magnitude lower. The VLBI-detected ETGs in this study are not preferentially more massive than their undetected counterparts and are typically drawn from relatively low density environments (i.e. are not the central galaxies of clusters). They also show significantly higher merger fractions (which are strictly lower limits, given the low depth of the SDSS images) than the general ETG population. Taken together, this suggests that a significant trigger for nearby radio AGN is galaxy merging.

Our analysis indicates that the onset of merger-triggered radio AGN is typically not prompt and takes place several dynamical time-scales into the starburst event, making it unlikely that the AGN provides strong regulation of this star formation. While the AGN may well couple to the remaining gas reservoir, the overall impact of this process will be to mop up residual gas, in a system where the gas reservoir has already been significantly depleted. As noted above, although these results are derived from a *GALEX*-detected subset of ETGs, they are representative of the nearby ETG population as a whole, making these results generally valid in the local Universe.

While the wider literature provides strong evidence for AGN feedback in systems where the black hole is fuelled by the cooling of hot gas (e.g. in central cluster galaxies), our results indicate that this is not the case when the gas is introduced into the system via a merger, at least at low redshift. The inability of the black hole to couple strongly to accreted gas then makes galaxy merging the dominant mode of stellar mass growth in nearby ETGs, precisely because the AGN is not able to regulate (and rapidly quench) merger-driven star formation. This scenario agrees with the recent literature which demonstrates widespread star formation in ETGs, which is indeed driven by minor mergers.

Finally, since the galaxies studied here are local, our results do not offer insight into the interaction of AGN with their host galaxies at high redshift. Given that the cosmic star formation and black hole accretion rates peak at $z \sim 2$, it is around these redshifts that the bulk of today's stellar mass must have formed and galaxy scaling relations, such as the $M_{\rm BH}$–σ correlation, largely put in place. As noted in Section 4, for these scaling relations to be established at high redshift over short time-scales, one requires a qualitatively different interaction between AGN and their hosts at these epochs. AGN in the early Universe must operate in normal LTGs and be triggered promptly in order to provide efficient regulation of star formation. While our local sample does not offer insight into AGN–galaxy coevolution at these epochs, similar studies at high redshift are keenly anticipated in order to probe the role of AGN in stellar mass growth around the epoch of peak cosmic star formation.

ACKNOWLEDGEMENTS

We are grateful to the anonymous referee for many constructive comments that improved the quality of the original manuscript. We thank Martin Hardcastle, Andrew King, Rachel Somerville, Frank van den Bosch, Meg Urry and Kevin Schawinski for interesting discussions. SK is grateful for support from the University of Tasmania (UTas) via a UTas Visiting Scholarship and acknowledges a Senior Research Fellowship from Worcester College Oxford. SSS acknowledges an ARC Early-Career Fellowship (DE130101399). ATD was supported by an NWO Veni Fellowship.

REFERENCES

Abazajian K. N. et al., 2009, ApJS, 182, 543
Alexander D. M., Swinbank A. M., Smail I., McDermid R., Nesvadba N. P. H., 2010, MNRAS, 402, 2211
Baan W. A., 2007, in Chapman J. M., Baan W. A., eds, Proc. IAU Symp. 242, Astrophysical Masers and their Environments. Cambridge Univ. Press, Cambridge, p. 437
Baldwin J. A., Phillips M. M., Terlevich R., 1981, PASP, 93, 5
Benson A. J., Bower R. G., Frenk C. S., Lacey C. G., Baugh C. M., Cole S., 2003, ApJ, 599, 38
Best P. N., Heckman T. M., 2012, MNRAS, 421, 1569
Best P. N., Kauffmann G., Heckman T. M., Ivezić Ž., 2005, MNRAS, 362, 9

Binney J., Tremaine S., 1987, Princeton Series in Astrophysics: Galactic Dynamics, 1st edn. Princeton Univ. Press, Princeton, NJ
Blanton M. R., Roweis S., 2007, AJ, 133, 734
Brinchmann J., Charlot S., White S. D. M., Tremonti C., Kauffmann G., Heckman T., Brinkmann J., 2004, MNRAS, 351, 1151
Calzetti D., Armus L., Bohlin R. C., Kinney A. L., Koornneef J., Storchi-Bergmann T., 2000, ApJ, 533, 682
Cappellari M. et al., 2012, Nature, 484, 485
Carpineti A. et al., 2012, MNRAS, 420, 2139
Cattaneo A. et al., 2009, Nature, 460, 213
Cen R., 2012, ApJ, 755, 28
Cole S., Lacey C. G., Baugh C. M., Frenk C. S., 2000, MNRAS, 319, 168
Cox T. J., Dutta S. N., Di Matteo T., Hernquist L., Hopkins P. F., Robertson B., Springel V., 2006, ApJ, 650, 791
Croton D. J. et al., 2006, MNRAS, 365, 11
Darg D. W. et al., 2010a, MNRAS, 401, 1043
Darg D. W. et al., 2010b, MNRAS, 401, 1552
Davies R. I., Müller Sánchez F., Genzel R., Tacconi L. J., Hicks E. K. S., Friedrich S., Sternberg A., 2007, ApJ, 671, 1388
Deller A. T., Middelberg E., 2014, AJ, 147, 14
Ellison S. L., Patton D. R., Mendel J. T., Scudder J. M., 2011, MNRAS, 418, 2043
Enßlin T. A., Gopal-Krishna2001, A&A, 366, 26
Fabian A. C., 1994, ARA&A, 32, 277
Fabian A. C., 1999, MNRAS, 308, L39
Fabian A. C., 2012, ARA&A, 50, 455
Fabian A. C., Nulsen P. E. J., Canizares C. R., 1982, MNRAS, 201, 933
Ferrarese L., Merritt D., 2000, ApJ, 539, L9
Gebhardt K. et al., 2000, ApJ, 543, L5
Granato G. L., De Zotti G., Silva L., Bressan A., Danese L., 2004, ApJ, 600, 580
Gültekin K. et al., 2009, ApJ, 698, 198
Haehnelt M. G., Natarajan P., Rees M. J., 1998, MNRAS, 300, 817
Hardcastle M. J., Evans D. A., Croston J. H., 2007, MNRAS, 376, 1849
Häring N., Rix H.-W., 2004, ApJ, 604, L89
Hatton S., Devriendt J. E. G., Ninin S., Bouchet F. R., Guiderdoni B., Vibert D., 2003, MNRAS, 343, 75
Hopkins P. F., 2012, MNRAS, 420, L8
Inskip K. J., Tadhunter C. N., Morganti R., Holt J., Ramos Almeida C., Dicken D., 2010, MNRAS, 407, 1739
Iwasawa K., Sanders D. B., Evans A. S., Trentham N., Miniutti G., Spoon H. W. W., 2005, MNRAS, 357, 565
Jahnke K., Macciò A. V., 2011, ApJ, 734, 92
Jeong H., Bureau M., Yi S. K., Krajnović D., Davies R. L., 2007, MNRAS, 376, 1021
Kauffmann G. et al., 2003, MNRAS, 341, 33
Kaviraj S., 2009, MNRAS, 394, 1167
Kaviraj S., 2010, MNRAS, 406, 382
Kaviraj S., 2014a, MNRAS, 437, L41
Kaviraj S., 2014b, MNRAS, 440, 2944
Kaviraj S. et al., 2007a, ApJS, 173, 619
Kaviraj S., Sohn S. T., O'Connell R. W., Yoon S., Lee Y. W., Yi S. K., 2007b, MNRAS, 377, 987
Kaviraj S., Rey S.-C., Rich R. M., Yoon S.-J., Yi S. K., 2007c, MNRAS, 381, L74
Kaviraj S., Kirkby L. A., Silk J., Sarzi M., 2007d, MNRAS, 382, 960
Kaviraj S. et al., 2008, MNRAS, 388, 67
Kaviraj S., Tan K.-M., Ellis R. S., Silk J., 2011a, MNRAS, 411, 2148
Kaviraj S., Schawinski K., Silk J., Shabala S. S., 2011b, MNRAS, 415, 3798
Kaviraj S. et al., 2013, MNRAS, 429, L40
Kaviraj S., Shabala S. S., Deller A. T., Middelberg E., 2015, MNRAS, preprint (arXiv:1412.5602)
Kewley L. J., Groves B., Kauffmann G., Heckman T., 2006, MNRAS, 372, 961
King A., 2003, ApJ, 596, L27
Komatsu E. et al., 2011, ApJS, 192, 18
Kondratko P. T. et al., 2006, ApJ, 638, 100
Koss M., Mushotzky R., Veilleux S., Winter L., 2010, ApJ, 716, L125
Ledlow M. J., Owen F. N., Yun M. S., Hill J. M., 2001, ApJ, 552, 120
Lintott C. J. et al., 2008, MNRAS, 389, 1179
Lonsdale C. J., Lonsdale C. J., Smith H. E., Diamond P. J., 2003, ApJ, 592, 804
Lonsdale C. J., Diamond P. J., Thrall H., Smith H. E., Lonsdale C. J., 2006, ApJ, 647, 185
McConnell N. J., Ma C.-P., Gebhardt K., Wright S. A., Murphy J. D., Lauer T. R., Graham J. R., Richstone D. O., 2011, Nature, 480, 215
McNamara B. R., Nulsen P. E. J., 2007, ARA&A, 45, 117
Madau P., Dickinson M., 2014, ARA&A, 52, 415
Magorrian J. et al., 1998, AJ, 115, 2285
Martin D. C. et al., 2005, ApJ, 619, L1
Morganti R., Fogasy J., Paragi Z., Oosterloo T., Orienti M., 2013, Science, 341, 1082
Morrissey P. et al., 2007, ApJS, 173, 682
Nenkova M., Sirocky M. M., Nikutta R., Ivezić Ž., Elitzur M., 2008, ApJ, 685, 160
Nesvadba N. P. H., Lehnert M. D., De Breuck C., Gilbert A. M., van Breugel W., 2008, A&A, 491, 407
Nesvadba N. P. H., Polletta M., Lehnert M. D., Bergeron J., De Breuck C., Lagache G., Omont A., 2011, MNRAS, 415, 2359
Nyland K. et al., 2013, ApJ, 779, 173
Oke J. B., Gunn J. E., 1983, ApJ, 266, 713
Pace C., Salim S., 2014, ApJ, 785, 66
Patton D. R., Pritchet C. J., Carlberg R. G. et al., 2002, ApJ, 565, 208
Peng C. Y., 2007, ApJ, 671, 1098
Robertson B., Bullock J. S., Cox T. J., Di Matteo T., Hernquist L., Springel V., Yoshida N., 2006, ApJ, 645, 986
Rupke D. S. N., Veilleux S., 2011, ApJ, 729, L27
Schawinski K., Thomas D., Sarzi M., Maraston C., Kaviraj S., Joo S.-J., Yi S. K., Silk J., 2007, MNRAS, 382, 1415
Schawinski K., Dowlin N., Thomas D., Urry C. M., Edmondson E., 2010, ApJ, 714, L108
Schlegel D. J., Finkbeiner D. P., Davis M., 1998, ApJ, 500, 525
Scott C., Kaviraj S., 2014, MNRAS, 437, 2137
Scudder J. M., Ellison S. L., Torrey P., Patton D. R., Mendel J. T., 2012, MNRAS, 426, 549
Shabala S., Alexander P., 2009, ApJ, 699, 525
Shabala S. S., Ash S., Alexander P., Riley J. M., 2008, MNRAS, 388, 625
Shabala S. S. et al., 2012, MNRAS, 423, 59
Silk J., Rees M. J., 1998, A&A, 331, L1
Sivia D. S., 1996, Data Analysis: A Bayesian Tutorial. Oxford Univ. Press, Oxford
Somerville R. S., Gilmore R. C., Primack J. R., Domínguez A., 2012, MNRAS, 423, 1992
Springel V., Di Matteo T., Hernquist L., 2005a, MNRAS, 361, 776
Springel V., Di Matteo T., Hernquist L., 2005b, ApJ, 620, L79
Strateva I. et al., 2001, AJ, 122, 1861
Sturm E. et al., 2011, ApJ, 733, L16
Tabor G., Binney J., 1993, MNRAS, 263, 323
Thomas D., Maraston C., Bender R., Mendes de Oliveira C., 2005, ApJ, 621, 673
Trager S. C., Faber S. M., Worthey G., González J. J., 2000, AJ, 119, 1645
Tremonti C. A. et al., 2004, ApJ, 613, 898
Veilleux S., Osterbrock D. E., 1987, ApJS, 63, 295
Wild V., Heckman T., Charlot S., 2010, MNRAS, 405, 933
Wyder T. K. et al., 2007, ApJS, 173, 293
Yang X., Mo H. J., van den Bosch F. C., Pasquali A., Li C., Barden M., 2007, ApJ, 671, 153
Yesuf H. M., Faber S. M., Trump J. R., Koo D. C., Fang J. J., Liu F. S., Wild V., Hayward C. C., 2014, ApJ, 792, 84
Yi S. K., 2003, ApJ, 582, 202
Yi S. K., Yoon S.-J., Kaviraj S. et al., 2005, ApJ, 619, L111
Young L. M., 2002, AJ, 124, 788

This paper has been typeset from a TEX/LATEX file prepared by the author.